Modeling and Characterization of Honeycomb Structures with Density Gradient Produced by Additive Manufacturing Technologies

Bernardo Capelo Coelho

Instituto Superior Técnico, Universidade de Lisboa, Portugal

November 2022

Abstract

Many technological advances have come from a close observation of nature, with cellular structures being a clear example of this. Honeycomb structures, a subsection of cellular materials, have gradually been implemented in many industrial sectors, as the associated high stiffness-to-weight ratio and energy absorption properties make them efficient lightweight alternatives to bulk materials. As a response to recent demands, an increase in studies regarding functional materials has surfaced, namely with density gradients being the highlighted tailorability factor regarding honeycomb structures. The present work is therefore a complementary investigation regarding functionally graded cellular materials, with its main objective being the mechanical characterization of regular and density graded honeycomb structures. Physical samples obtained via additive manufacturing were experimentally submitted to compression testing, along with a computational model of the test being developed using the finite element method (FEM). Specific stiffness and absorbed energy were analysed, with the variation of these properties with relative density and apparent area also being recorded.

Overall, the functionally graded structures showed better mechanical performance when compared to their regular counterparts. In terms of out-of-plane testing, graded structures showed higher values for stiffness, with the main influence factor being the apparent area. In terms of in-plane testing, graded structures exhibited superior energy absorption than their regular counterparts, with relative density being the main driver. The in-plane numerical results showed an acceptable correlation with the experimental results, with satisfactory matching in plastic deformation and failure.

Keywords: Functionally Graded Cellular Structures; Honeycomb Structures; Finite Element Method; Compression Testing; Additive Manufacturing; Density Gradient.

1. Introduction

Cellular materials have been a studying subject for countless years due to their high stiffness-to-weight ratio and energy absorption properties, acting as excellent alternatives for heavier bulk materials in structural applications. One of the originally studied cellular structures was the honeycomb structure, dating up to the two millennia ago [1]. Although these structures are predominantly employed as core materials in sandwich panels, making use of their excellent out-of-plane stiffness and strength, there is a growing interest in exploring their in-plane mechanical properties, mainly in terms of energy absorption [2] [3].

Due to the constant technological advances seen in recent years, there was a growing need of functionally adapted structures which could respond specifically to certain applications, leading to the development of functionally graded cellular structures. The evolution of additive manufacturing technologies further aided in the implementation of these structures in the majority of industry sectors, as more complex geometries could be produced in various materials. Although numerous types of gradients can be implemented in functionally graded honeycomb structures, like composition gradients, the mostly studied are density gradients, in which relative density is altered throughout the structure by variating different geometric parameters (e.g., cell wall thickness, periodicity of unit cell, cell wall length). Liu et al. (2021) [4]studied the use of sequentially repeating smaller hexagonal unit cells in different layer levels of honeycomb structures, making use of fractal self-similarity in order to vary the relative density of the structure throughout its length, observing an increase in energy absorption of around 89% in low-velocity impact and 17% in high-velocity impact. Liu et al. (2022) [5] further studied the use of density gradients in the crashworthiness performance of honeycomb structures by implementing a hierarchical topology to these structures. In this study, cell walls were themselves comprised of regular hexagonal and triangular honeycomb unit cells of different sizes, gradually varying the relative density along its length, obtaining an increase in specific absorbed energy of around 32% when compared to regular honeycomb structures. These functionally graded structures have a wide range of applications, ranging from aerospace to automotive industries, being even applied in the defence industry [6] [7].

The present study aims towards contributing to the research of the mechanical behaviour of functionally graded honeycomb structures, more specifically density graded honeycomb structures. With this objective in mind, different regular and graded aluminium honeycomb structures were subjected to compression testing (both experimentally and numerically), ultimately having as its main objective the identification of relevant geometric parameters and the assessment of differences in mechanical response with differing designs.

2. Materials and Methods

2.1 Materials

The samples tested experimentally were produced via the selective laser melting (SLM) process, of which the metallic powder used was the alloy AlSi7Mg0.6, an aluminium cast alloy described as EN AC-42200 by the standard DIN EN 1706 [8], produced by the SLM Solutions Group, of which physical and mechanical properties can be found in table 1. Although this aluminium alloy was originally used in casting applications, it has been gradually incorporated in additive manufacturing processes due to its satisfactory corrosion resistance and weldability.

Table 1. AlSi7Mg0.6 properties [9]

Density [g/cm³]	2.680
Young’s Modulus [MPa]	59000
Poisson’s Ratio	0.33

2.2 Structure Design

The structures studied in the present work can be divided into regular and graded. Three different sets of regular structures were designed depending on the cell wall length (l), which took the values of 6mm, 8mm, and 10mm, as presented in figure 1. For every design with a set value of cell wall length, the cell core height (h) was varied between 6mm, 10mm and 12mm, obtaining a total of 9 different structures. The cell wall thickness (t) was kept constant at 2.31mm. These structures are referred to depending on their values for cell wall length and cell core height, with a hypothetical structure with l =6mm and h =6mm being attributed the designation *L6H6*.

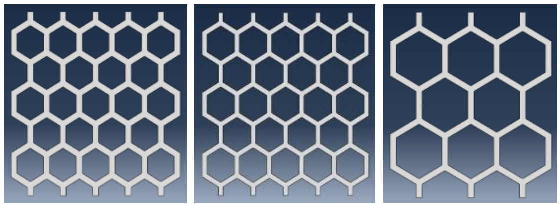

(a) (b) (c)

Figure 1. 3D-CAD model for structures: (a) L6; (b) L8; (c) L10.

The graded structures were designed as in the previous work by Rua (2021) [10], according to three different gradient types, with a total of 12 different structures of constant core cell height (12mm). Due to the typical radial symmetry of honeycomb geometry, the density gradient was propagated in equally distanced concentric circumferences centred in the centre of the structure, as exemplified in figure 2. The designation for each graded structure depends on its gradient group, with the examples of the first and second structures designed with gradient *1* being assigned the designation *1A* and *1B*, respectively. The same applies to the remaining gradient types.

Two structures were designed according to gradient *1*, in which the design depended on

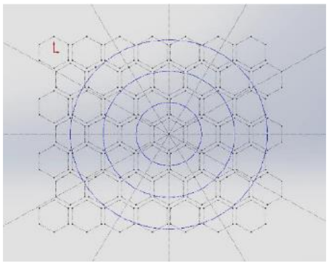

Figure 2. Main symmetry lines and exemplification of associated concentric circumferences.

fixed values of cell wall length, with cell wall thickness varying as a function of the previous parameter: one with increasing cell length ($l: 6 \rightarrow 8 \rightarrow 10$) and consequent decreasing cell wall thickness, and one with decreasing cell length ($l: 10 \rightarrow 8 \rightarrow 6$) and consequent increasing cell wall thickness.

Regarding gradient *2*, four structures were designed. This gradient type is once again dependent on cell wall length, with this parameter varying between 7mm and 9mm in increasing and decreasing density gradients. For decreasing gradient, the centre cell was designed with a cell wall length of 7mm, progressively increasing by an increment of 0.5mm with each concentric circumference. Two different structures were developed with this grading, differing solely on the cell wall length of the four cells in the corners (either 7mm or 8.5mm). For increasing gradient, the centre cell wall was designed with a cell wall length of 9mm, progressively decreasing by an increment of 0.5mm with each concentric circumference. With the same criterion of the previously gradient, two different structures were developed (either 7.5mm or 8.5mm).

Six structures were design according to gradient *3*, which is based on a gradient parameter R, calculated according to certain geometric variables, as presented in figure 3 (a). This parameter is extrapolated from the initial and final values chosen for cell wall thickness and a relative cell length, as shown in figure 3 (b), with the density gradient emerging as a consequence of this variation. Positive R parameters indicate a decrease in relative density from centre to exterior, while negative R parameters indicate the opposite, with higher module values of parameter R meaning steeper gradients. It is important to refer that in order to maintain coherence in the present work, cell wall thickness of an i cell should be referred as t_i.

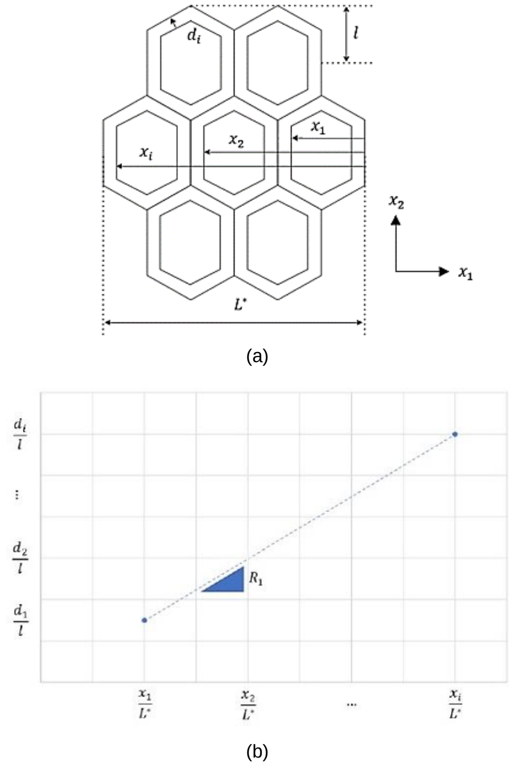

Figure 3. (a) Designation of variables involved in the definition of (b) the gradient parameter R.

Examples of designs for each gradient are shown in Figure 4, with designations and important geometrical parameters for both regular and graded structures displayed in Tables 2 and 3, respectively.

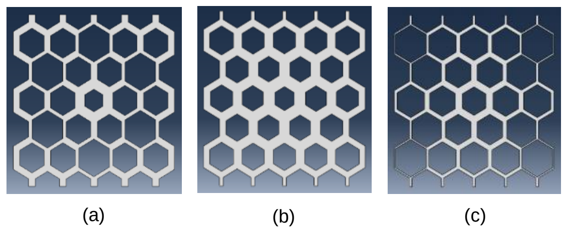

Figure 4. 3D-CAD model for structures: (a) 1A; (b) 2A; (c) 3C(+).

Table 2. Designation and geometrical parameters for the regular structures.

Code	h [mm]	l [mm]	Apparent Area [mm^2]	$\bar{\rho}$
L6H6	6			
L6H10	10	6	65.81 × 66 (4343.46)	0.338
L6H12	12			
L8H6	6			
L8H10	10	8	83.15 × 84 (6984.60)	0.269
L8H12	12			
L10H6	6			
L10H10	10	10	61.20 × 68 (4161.60)	0.228
L10H12	12			

Table 3. Designation and geometrical parameters for graded structures.

Code	l change [mm]	R	Apparent Area [mm^2]	$\bar{\rho}$
1A	6 → 8 → 10	---	91.59 × 91.35 (8366.47)	0.322
1B	10 → 8 → 6	---		0.421
2A	7+0.5(8.5)*	---		0.443
2B	7+0.5 (7)*	---	100.46 × 102 (10246.92)	0.466
2C	9-0.5 (7.5)*	---		0.426
2D	9-0.5 (8.5)*	---		0.410
3A(+)	---	+0.22		0.323
3A(-)	---	-0.22		0.240
3B(+)	---	+0.31	88.51 × 90 (7965.90)	0.265
3B(-)	---	-0.31		0.298
3C(+)	---	+0.37		0.199
3C(-)	---	-0.37		0.335

*Values between brackets indicate the cell wall length of corner cells.

2.3 Manufacturing

The additive manufactured samples tested in the present study were produced via SLM, in a SLM Solutions 125HL machine belonging to the École Nationale Supérieure des Mines d'Albi-Carmaux, in France. The previously mentioned machine possesses a single laser of 400W, with possible width ranging from 70μm to 100μm and a maximum speed of 10m/s, using argon as an inert gas. For the tested samples, single layers of powder aluminium alloy (AlSi7Mg0.6) were fused sequentially, with thickness ranging from 20μm to 75μm. Every regular geometry was manufactured, with only three graded structures being produced: *2D*, *3A(-)* and *3B(+)*.

2.4 Finite Element Modeling

The compression testing simulations were performed using the finite element analysis (FEA) software *ABAQUS 2022*, by Dessault Systèmes S.A. The regular structures were designed withing this software, with the 3D-CAD of the graded structures imported as .IGS files. Two additional cylindrical parts with a radius of 70mm and height of 10mm were designed, to serve as the compression plates in the simulated testing. These parts were assigned the material "*Rigid"*, defined as purely elastic and with a Young's modulus several orders of magnitude above the one of the aluminium alloy (E=1E+15MPa) and an exceptionally low Poisson's ratio (υ = 0.0001) to ensure the deformation in the system is purely induced in the studied structures. A second material *"Aluminium"* was created, to which were assigned the physical and mechanical properties described in Table 1 for the elastic section, with the true values for the yield stress and strain and the ultimate stress and respective strain being given to the software to the describe its plastic behaviour.

The interaction in the contact surfaces between the compression plates and the tested structures was defined as having a friction coefficient of 0.2. The lower compression plate was fixed using the command *Encastre*, denying any rotational or translational movement, with the upper compression plate being assigned a displacement of 1.5mm in out-of-plane testing and 3mm in in-plane testing.

The specimens were meshed using a ten-node quadratic tetrahedral element type (C3D10), with a larger global seed size of 8mm being chosen for the compression plates to reduce the computational load of the simulations. A convergence analysis was performed regarding the regular and graded honeycomb structures, ensuring the ideal number of elements while maintaining the computational process time balanced and consequently verifying the quality of the mesh. The evolution of the average von Mises stress was recorded in three fixed nodes over a number of different meshes, reaching the conclusion that the ideal mesh size was 1.4mm for both regular and graded structures, corresponding to a number of elements of 34742 and 132588, respectively. An example of the assembly in the visualization module is shown in Figure 5.

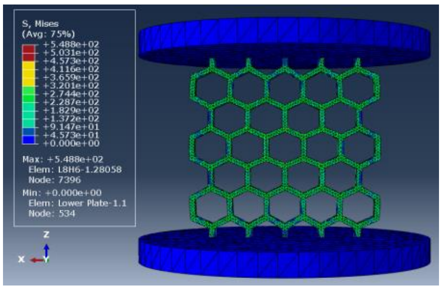

Figure 5. Visualization module (deformed L8H6 sample with parameter average von Mises stress).

The requested output variables were the displacement and reaction forces, observed in the moveable compression plate, which allowed for the calculation of the force-displacement curves. From these curves, two properties were calculated: the stiffness K, i.e. the slope of the linear region of the curves and the absorbed energy E_a, i.e. the surface below the curves until a certain displacement (0.7mm and 1.5mm for out-of-plane and in-plane testing, respectively). By dividing these properties by the relative density, the specific values were obtained. Additionally, the von Mises stress was requested in order to ascertain stress levels and compare its magnitude between structures, as well as the plastic strain, which allowed for the observation of permanent deformation after unloading.

2.5 Experimental Testing

The experimental compression tests were performed according to the ASTN C365-94 standard [11], in an Instron 3369 universal mechanical testing machine, equipped with a load cell of 50kN, as shown in Figure 6. Both out-of-plane and in-plane tests were performed with a constant displacement rate of 0.5mm/min. Testing was carried out until failure points were clearly visible, so the failure mechanics could later be analysed. The data was processed via the *Instron Bluehill Universal* software, and later treated into force-displacement curves. As in the numerical simulations, stiffness (K) and absorbed energy (E_a) were calculated. The deformed samples were then observed via a low-resolution stereomicroscope, aiming for a better understanding of the failure mechanisms.

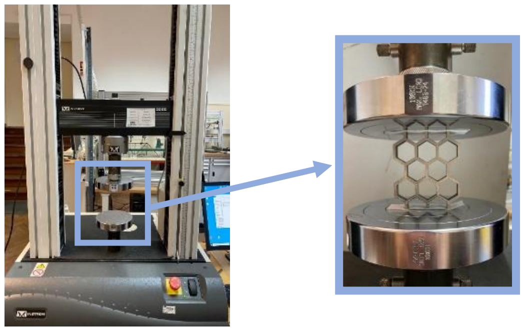

Figure 6. Compression testing machine apparatus (Instron 3369).

3. Results

3.1 Numerical Results

Table 4 and 5 show the values of specific stiffness and specific absorbed energy calculated via the force-displacement curves obtained in the in-plane simulations of regular and graded structures, respectively.

Table 4. Specific stiffness and specific absorbed energy for regular structures (in-plane).

Code	$\overline{\rho}$	Area [mm^2]	$\overline{K}$ [kN/mm]	$\overline{E_a}$ [J]
L6H10	0.338	4343.46	108.6	63.9
L8H10	0.269	6984.60	70.7	50.8
L10H10	0.228	4161.60	40.1	27.9

Table 5. Specific stiffness and specific absorbed energy for graded structures (in-plane).

Code	$\overline{\rho}$	Area [mm^2]	$\overline{K}$ [kN/mm]	$\overline{E_a}$ [J]
1A	0.322	8366.47	91.2	63.0
1B	0.421		166.9	101.5
2A	0.443	10246.92	195.1	114.1
2B	0.466		214.0	121.1
2C	0.426		195.1	123.7
2D	0.410		178.9	116.4
3A(+)	0.323	7965.90	91.4	85.8
3A(-)	0.240		57.5	42.3
3B(+)	0.265		86.3	59.5
3B(-)	0.298		82.5	55.7
3C(+)	0.199		49.2	34.0
3C(-)	0.335		100.3	65.4

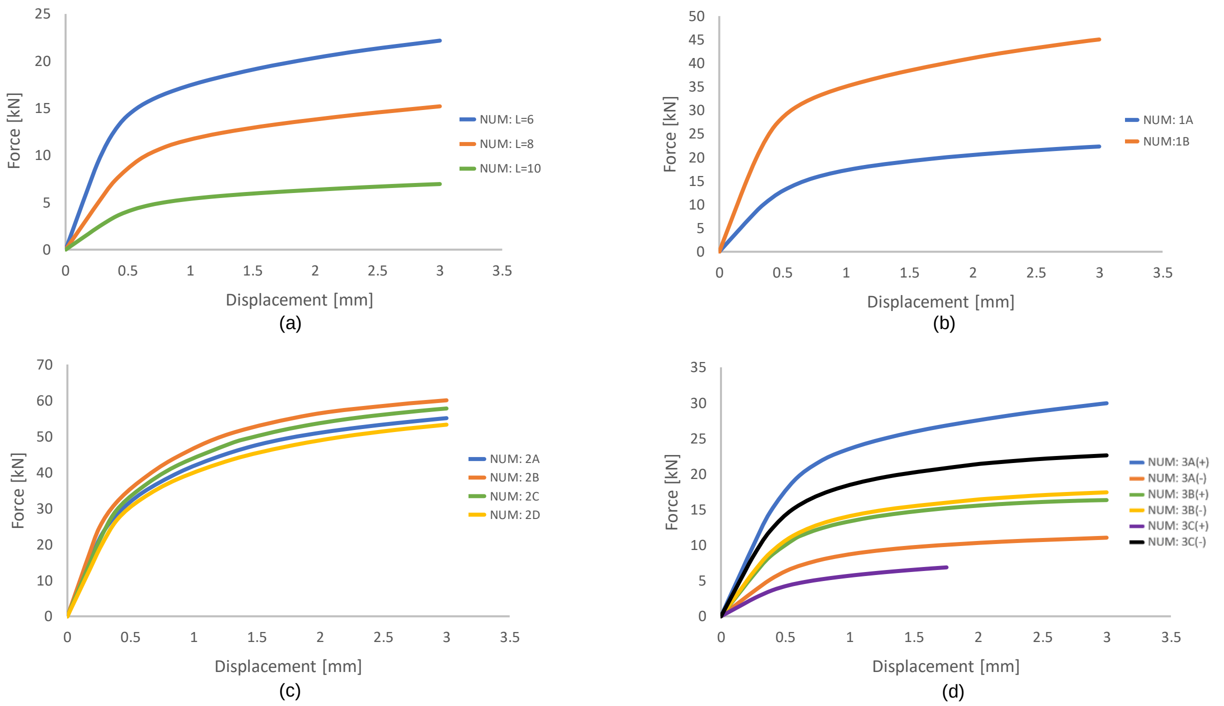

Figure 7. Numerical force-displacement curves for (a) regular structures and graded structures based on (b) gradient *1*, (c) gradient *2*, (c) gradient *3*.

The previously mentioned force-displacement curves are shown in Figure 7, distributed into (a) regular structures, (b) gradient type *1*, (c) gradient type *2* and (d) gradient type *3*. An observation of the force-displacement curves regarding the regular structures (Figure 7 (a)) allows for the conclusion that the in-plane mechanical performance is influenced by the cell wall length, and consequently the relative density. Lower cell wall length values (higher relative density) are translated into higher values of specific stiffness and specific absorbed energy, as shown in Table 4, with the structure *L6H10* being the best performing. Regarding the graded structures, the same overall behaviour is identified, with minimal variations. The best performing structures were the ones designed with gradient *2*, characteristically presenting the highest values of relative density, showing the highest values of specific stiffness and specific absorbed energy being recorded. There are some variations within the mechanical performance of the structures designed with gradient *3*, e.g. structure *3B(+)* exhibits a lower relative density than structure *3B(+)* but showed higher values for both specific stiffness and specific absorbed energy, which is an indicator that more complex gradients can be studied in order to achieve better mechanical properties with lower material use.

Regarding the out-of-plane numerical results, a pattern is visible when analysing Figure 8, with specific stiffness increasing almost linearly with the apparent area. Once again, the structures designed with gradient *2* were the best performing, with graded structures showing higher values of specific stiffness when compared with the regular structures (higher specimen size).

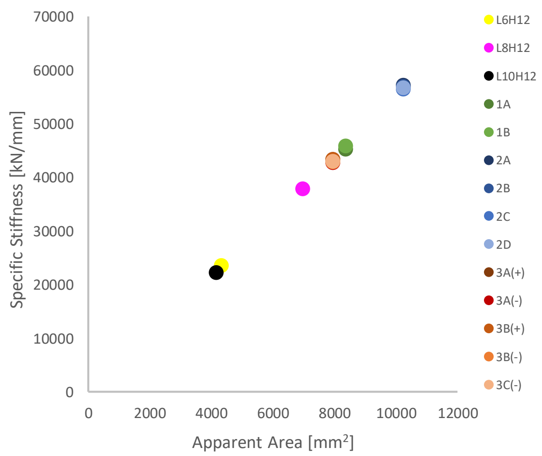

Figure 8. Out-of-plane specific stiffness vs apparent area (regular and graded structures).

3.2 Experimental Results

Figure 9 shows the experimental force-displacement curves obtained for the regular and graded tested structures compared to the corresponding numerical curve, more specifically for the structures (a) *L6H10*, (b) *L8H10*, (c) *L10H10*, (d) *2D*, (e) *3A(-)* and (f) *3B(+)*. The mechanical properties calculated from the previously mentioned curves, namely specific stiffness and specific absorbed energy, are showed in Table 6, ordered by increasing relative density. Both regular and graded experimental curves are relatively close to the corresponding numerical, which suggests a good approximation of the computational model. The same is relatively observed for the calculated mechanical properties, with some variations, that can be attributed to the

Table 6. Experimental and numerical results for specific stiffness and specific absorbed energy.

			Numerical		Experimental	
Code	$\overline{\rho}$	**Area [mm^2]**	$\overline{K}$ **[kN/mm]**	$\overline{E_a}$ **[J]**	$\overline{K}$ **[kN/mm]**	$\overline{E_a}$ **[J]**
L10H10	0.228	4161.60	40.1	27.9	25.8	21.1
3A(-)	0.240	7965.90	57.5	42.3	33.5±2.3	29.5±2.1
3B(+)	0.265	7965.90	86.3	59.5	43.7±2.2	36.8±2.9
L8H10	0.269	6984.60	70.7	50.8	38.9	36.1
L6H10	0.338	4343.46	108.6	63.9	48.8	44.3
2D	0.410	10246.92	178.9	116.4	55.4±3.0	50.5±3.6

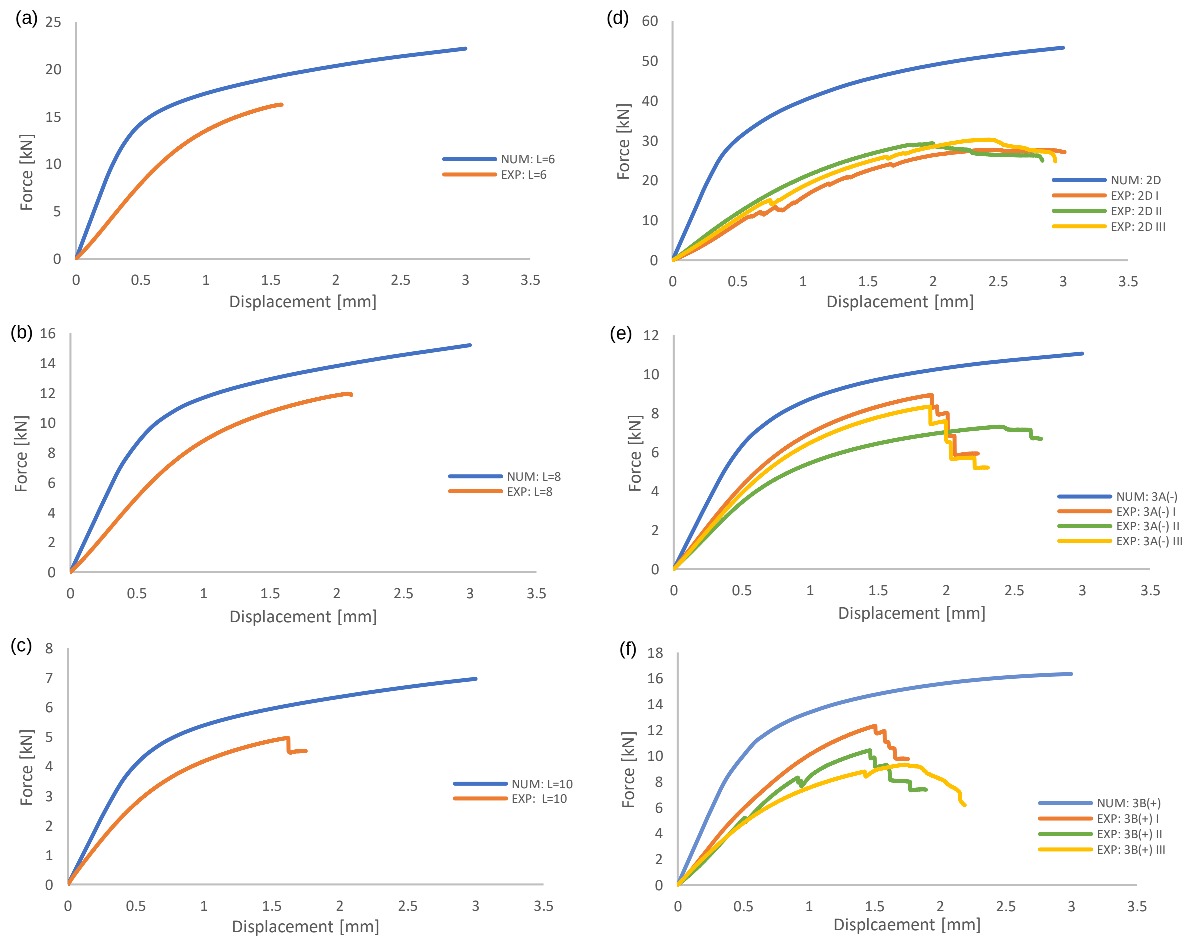

Figure 9: Experimental and numerical force-displacement curves for structures (a) *L6H10*; (b) *L8H10*; (c) *L10H10*; (d) *2D*; (e) *3A(-)*; (f) *3B(+)*.

presence of solid porosity and an irregular topography in the experimental specimens, contrary to the simulated ones (virtually no defects). The experimental values presented in Table 6 also show the previously described pattern, with increasing relative density being translated into an increase in both specific stiffness and specific absorbed energy. Figure 10 facilitates the comparison between regular and graded structures regarding the analysed experimental mechanical properties. A comparison between the pairs *L10H10*/*3A(-)* and *L8H10*/*3B(+)* shows how the graded structures perform better in terms of energy absorbing and stiffness when compared with regular structures of extremely similar relative density

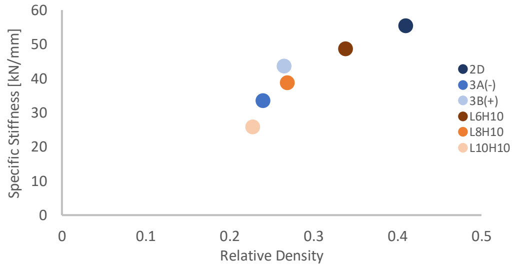

(a)

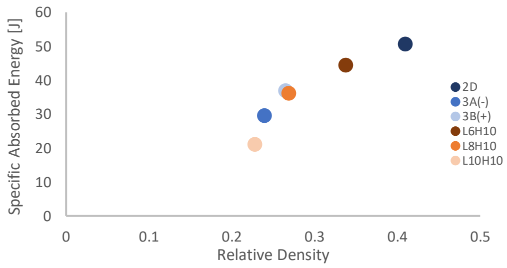

(b)

Figure 10. Experimental in-plane (a) specific stiffness and (b) specific absorbed energy with relative density.

3.3 Failure Analysis

Figures 11 and 12 show the matching the permanent deformation withstood by the specimens *L8H10* and *3B(+)*, respectively. In both the regular and graded cases (Figure 11 and 12, respectively), plastic strain is mainly concentrated in the structures' triple junctions, points in which three cell walls are joined, consequently becoming stress concentrating regions. Regarding the regular structure (*L8H10*), the regions in which plastic strain is more accentuated are around the centre of the structure, for both numerical and experimental

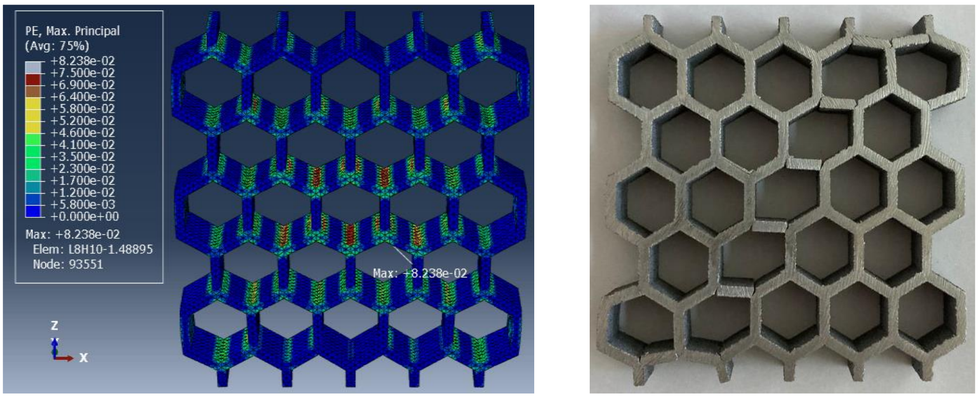

Figure 11. In-plane simulated (maximum plastic strain, PE) and experimental deformed samples for *L8H10* structure.

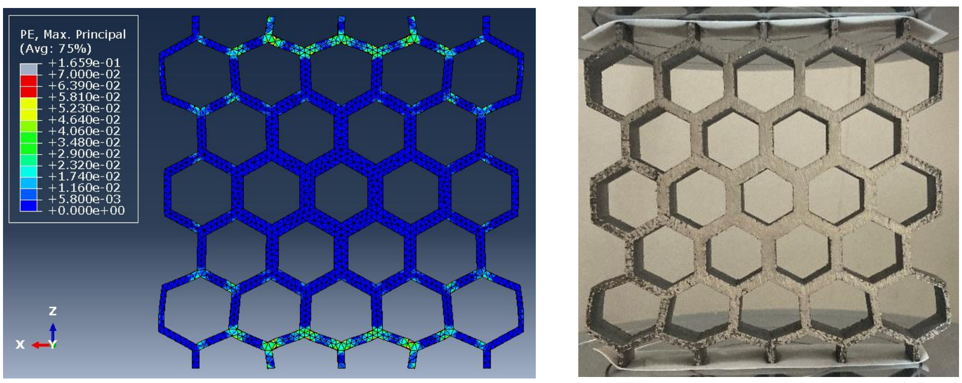

Figure 12. In-plane simulated (maximum plastic strain, PE) and experimental deformed sample for *3B(+)* structure.

cases, with a relatively uniform decreasing of intensity in the radial direction. The plastic strain observed in the graded structure model is concentrated predominantly around the upper and lower middle contact regions between the structure and the compression plate, coinciding with the regions in which cell wall thickness is lower. The same is observed in the experimentally deformed specimen (solely on the lower contact region), with coinciding buckling of the lower exterior cell walls. For the same displacement (3mm), the graded structure was still structurally intact when compared to the regular structure, further suggesting the advantages of functionally graded structures. This is corroborated by the values presented in Table 6, as the sample *L8H10*, which presents a higher relative density than the sample *3B(+)*, should present higher values of stiffness and absorbed energy, with the opposite being observed.

Figure 13 shows the magnified vision of one of the collapsed cells in sample *L6H10*, in which the origin of the fracture can be attributed to a crack initiated in the surface of a junction of three cell walls. This crack is divided into two subsequent cracks which propagate in the direction of the remaining two contact points between cell walls, further confirming how stresses are concentrated in these geometrical changes. The irregular topography of the exterior of the cell walls is another factor which influences crack initiation and propagation.

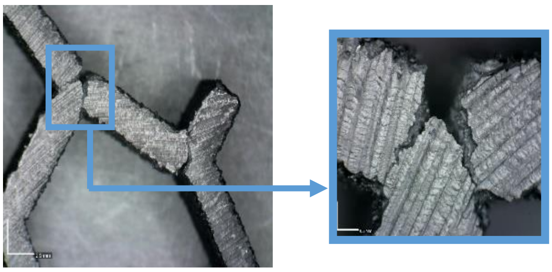

Figure 13. Fracture of a collapsed cell with magnification 0.5x and 2x (sample *L6H10*).

The surface of a fractured cell was also observed, as shown in Figure 14, providing additional information regarding the macrostructure of the additive manufactured metal. A close observation of the fracture surface presented in Figure 13 allows for the identification of some level of porosity in the solid walls, possibly due to the presence of hydrogen during the fabrication process, which originates from residual humidity. Additionally, this type of microstructure is associated with the possible presence of inclusion, which might be attributed to an isolated separation of a silicon-rich phase consequent of the additive manufacturing process [12].

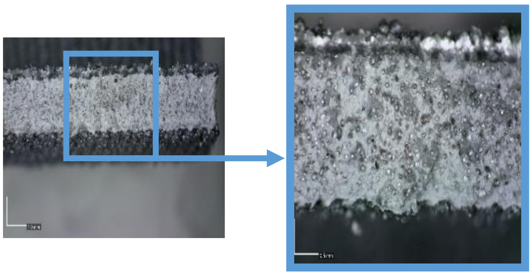

Figure 14. Fracture surface resulting from a fractured triple junction with magnification 0.5x and 2x (sample *L8H10*).

4. Conclusions

The present work aimed for the mechanical characterization of regular and functionally graded honeycomb structures produced via selective laser melting, allowing for the identification of promising designs using density gradients, as well as influential geometrical parameters. The samples were experimentally submitted to compression tests, with a computational model of the same tests being developed using the Finite Element Method. A satisfactory correlation between the numerical and experimental results was obtained, namely in the in-plane orientation, with similar numerical and experimental force-displacement curves and matching plastic deformation. It was concluded that the relative density and apparent area were the most influential geometrical parameters: regarding out-of-plane testing, an increase in apparent area was translated into an increase in both specific stiffness and specific absorbed energy, with the same pattern being observed with relative density regarding in-plane testing. The best performing structures were the ones designed with gradient *2*, in which the gradient is dependent on cell wall length, with this parameter varying between 7mm and 9mm in increasing or decreasing density gradients. Overall, mechanical performance was superior for graded structures when compared with regular structures of similar size and relative density, further suggesting the relevance of functionally graded structures. Finally, a failure analysis was performed on the deformed regular structures, analysing the regions in which plastic deformation was mostly concentrated (triple junctions). The fracture surface of a collapsed cell was analysed, revealing defects typical of parts produced by additive manufacturing, like some level of solid porosity due to residual humidity during the fabrication process.

References

[1] T. C. Hales, "The honeycomb conjecture," *Discrete Comput Geom*, vol. 25, no. 1, pp. 1–22, 2001, doi: 10.1007/s004540010071.

[2] X. Wei, D. Li, and J. Xiong, "Fabrication and mechanical behaviors of an all-composite sandwich structure with a hexagon honeycomb core based on the tailor-folding approach," *Compos Sci Technol*, vol. 184, Nov. 2019, doi: 10.1016/j.compscitech.2019.107878.

[3] T. Fan, "Dynamic crushing behavior of functionally graded honeycomb structures with random defects," *International Journal of Materials Research*, vol. 107, no. 9, pp. 783–789, Sep. 2016, doi: 10.3139/146.111403.

[4] H. Liu, E. T. Zhang, and B. F. Ng, "In-plane dynamic crushing of a novel honeycomb with functionally graded fractal self-similarity," *Compos Struct*, vol. 270, p. 114106, Aug. 2021, doi: 10.1016/j.compstruct.2021.114106.

[5] H. Liu, E. T. Zhang, G. Wang, and B. F. Ng, "In-plane crushing behavior and energy absorption of a novel graded honeycomb from hierarchical architecture," *Int J Mech Sci*, vol. 221, p. 107202, May 2022, doi: 10.1016/j.ijmecsci.2022.107202.

[6] P. Zhou, L. Huang, J. Xie, D. Liang, H. Lu, and L. Deng, "Prediction of Microwave Absorption Behavior of Grading Honeycomb Composites Based on Effective Permittivity Formulas," *IEEE Trans Antennas Propag*, vol. 63, no. 8, pp. 3496–3501, Aug. 2015, doi: 10.1109/TAP.2015.2431721.

[7] R. Qin, J. Zhou, and B. Chen, "Crashworthiness Design and Multiobjective Optimization for Hexagon Honeycomb Structure with Functionally Graded Thickness," *Advances in Materials Science and Engineering*, vol. 2019, pp. 1–13, Feb. 2019, doi: 10.1155/2019/8938696.

[8] Deutsches Institut für Normung, "DIN EN 1706: Aluminium and aluminium alloys - Castings - Chemical composition and mechanical properties," 1998.

[9] SLM Solutions Group AG, "Al-Alloy AlSi7Mg0,6 Material Data Sheet."

[10] T. Rua, "Out-of-Plane Compression Behaviour of Honeycomb Structures with Mass Gradient Produced by Additive Manufacturing Technologies," Masters, Instituto Superior Técnico, Universidade de Lisboa, Lisbon, 2021.

[11] "Standard test method for flatwise compressive properties of sandwich cores," *ASTM C365-94*.

[12] Z. W. Xu, Q. Wang, X. S. Wang, C. H. Tan, M. H. Guo, and P. B. Gao, "High cycle fatigue performance of AlSi10mg alloy produced by selective laser melting," *Mechanics of Materials*, vol. 148, p. 103499, Sep. 2020, doi: 10.1016/j.mechmat.2020.103499.